



Highly efficient and green chemical synthesis of imidazolyl alcohols and N-imidazolyl functionalized β -amino compounds using nanocrystalline ZSM-5 catalysts



Rajkumar Kore^a, Biswarup Satpati^b, Rajendra Srivastava^{a,*}

^a Department of Chemistry, Indian Institute of Technology Ropar, Rupnagar 140001, India

^b Saha Institute of Nuclear Physics, 1/AF, Bidhannagar, Kolkata 700064, India

ARTICLE INFO

Article history:

Received 22 January 2014

Received in revised form 28 February 2014

Accepted 3 March 2014

Available online 13 March 2014

Keywords:

Nanocrystalline zeolites

Zirconosilicates

Imidazolyl alcohols

Aminolysis

Hydroamination

ABSTRACT

A solvent free protocol is developed for the synthesis of imidazolyl alcohols and N-imidazolyl functionalized β -amino compounds. Imidazolyl alcohols were synthesized by the ring opening of epoxides with imidazoles and N-imidazolyl functionalized β -amino compounds were synthesized by the hydroamination reaction of imidazoles and activated olefins. These reactions were catalyzed by a variety of crystalline heterogeneous catalysts such as Al/Zr substituted nanocrystalline ZSM-5 (M-Nano-ZSM-5), conventional M-ZSM-5 (where M = Zr, Al), and Zr substituted amorphous mesoporous catalysts (Zr-SBA-15 and Zr-KIT-6). Among these catalysts, nanocrystalline Zr-Nano-ZSM-5 exhibited the highest activity and regioselectivity. Structure activity relationship is explained based on the catalytic activity, acidity measurements, reactivity of reactants (imidazoles/epoxides/methyl acrylate), competitive adsorption, nature, and type of catalysts. Zr-Nano-ZSM-5 exhibited exceptionally high catalytic activity compared to the catalysts reported in the literature for the synthesis of imidazolyl alcohols and other imidazole derivatives.

© 2014 Elsevier B.V. All rights reserved.

1. Introduction

Heterocyclic compounds are building blocks of many biologically important molecules such as deoxyribonucleic acid, hemoglobin, chlorophyll, proteins etc. Heterocyclic compounds are synthetic intermediates for the production of agrochemicals, drugs, insecticides, herbicides, etc. [1]. 1,3-diazoles (imidazole derivatives) are important heterocyclic synthetic precursor [2–4]. Among imidazole derivatives, imidazolyl alcohols are one of the important building blocks for the synthesis of antiprotozoal (metronidazole, ornidazole, and secnidazole) and antifungal drugs (miconazole and econazole) [5]. Compounds containing imidazole moiety play important roles in the green chemistry and catalysis. Most of the commercial ionic liquids and ionic liquids based research are based on imidazole. Because of the functionalization ability of imidazole ring, a wide range of ionic liquids were prepared and investigated in the catalytic reactions [6–9]. Imidazole based ligands are known to make a wide range of homogeneous complexes [10,11]. These

complexes can be supported or encapsulated in the mesoporous material for efficient recycling [12].

Several routes are known for the synthesis of imidazolyl alcohols that include N-alkylation of imidazole and ring opening of epoxides with imidazole [13–18]. Among these, ring opening of epoxide with imidazole nucleophile is the best synthetic route [14–18]. Epoxides are three-member heterocyclic ring that are more reactive than ethers due to ring strain. When nucleophiles attack the electrophilic C of the C–O bond, ring opening of epoxide takes place due to the cleavage of C–O bond of epoxide. Ring opening of epoxide with imidazole nucleophile is either un-catalyzed (but occurs at very high temperature and high pressure) or catalyzed by acid or base catalysts [14–18]. Catalysts reported for this reaction are suffered from several disadvantages such as high pressure, high temperature, longer reaction time (7 days), use of solvent, use of excess amount of expensive reagents or catalysts, use of microwave radiation, and in-efficient recycling of the catalyst. Very recently, a three-step synthetic route is reported for the preparation of imidazolyl alcohol, which involves: (a) silylation of imidazole, (b) ring-opening of epoxide with silylated imidazole catalyzed by LiBr, and (c) desilylation with KF [18]. Imidazole derivatives can also be synthesized by the hydroamination reaction of imidazole and activated olefins using the acid/base catalysts [19–31].

* Corresponding author. Tel.: +91 1881 242175; fax: +91 1881 223395.

E-mail addresses: rajendra@iitrpr.ac.in, [\(R. Srivastava\).](mailto:chemi.rajendra@yahoo.co.in)

Catalysts reported for this reaction are suffered from one or more disadvantages such as longer reaction time (24 h), use of solvent, use of excess amount of expensive reagents or catalysts, and inefficient recycling of the catalyst. Therefore, it is very important to develop one-step, economical, and reusable catalyst based synthesis methodology for the preparation of imidazolyl alcohols and other imidazole derivatives.

Our research is focused on the synthesis of ionic liquid and zeolite based catalysts and finds their applications in the selective synthesis of important organic molecules. Among the ionic liquid and zeolite based catalysts, zeolite based catalysis is more attractive due to user-friendliness, easy recovery, and recyclability. Zeolites have been given significant attention due to their acidic properties, shape selectivity, and redox properties (obtained by the isomorphous substitution of transition metal ions in the framework) [32–34]. However, the application of conventional zeolite is limited in the synthesis of large organic molecules due to the pore diffusion limitations. To overcome this problem, our group and other catalysis/material scientists have developed synthesis strategies for the preparation of nanocrystalline zeolites having inter/intra-crystalline mesopores that enhance the diffusion of reactant/product molecules and improve the lifetime of catalyst [35–46]. A variety of ionic/non-ionic/polymeric soft templates and hard templates (based on silica and carbon materials) have been reported for the synthesis of nanocrystalline zeolites [42–46].

In this study, one-step, eco-friendly, solvent free catalytic route is reported for the synthesis of imidazolyl alcohols using Al/Zr containing nanocrystalline ZSM-5 catalysts (hereafter represented as M-Nano-ZSM-5, where M = Al, Zr) (**Scheme 1**). Application of these catalysts is extended in the synthesis of other imidazole derivatives by the hydroamination reaction of imidazole and activated olefin (**Scheme 1**). For comparative study, microporous ZSM-5 catalysts (M-ZSM-5) and amorphous mesoporous zirconosilicates (such as Zr-SBA-15 and Zr-KIT-6) were also investigated. Zr-Nano-ZSM-5 exhibited exceptionally high catalytic activity compared to the catalysts reported in the literature for the synthesis of imidazolyl alcohols and other imidazole derivatives.

2. Experimental

2.1. Material preparation

2.1.1. Synthesis of nanocrystalline ZSM-5 catalysts

In a typical synthesis of Zr-Nano-ZSM-5, required amount of zirconium (IV) isopropoxide (ZrIPO) was added to 23.72 g of tetraethylorthosilicate (TEOS) and the resultant solution was stirred for 15 min under ambient condition until reaction mixture becomes clear solution (Solution A). PrTES (PrTES = propyl triethoxy silane) (1.74 g) was mixed with TPAOH (42.7 g) to form solution B. Solution A was added slowly to the solution B, followed by the addition of 52 mL of distilled water. The resultant gel was further homogenized for 3 h under stirring. The reaction mixture was transferred to a Teflon-lined stainless steel autoclave, and hydrothermally treated at 443 K for 5 days under static conditions. The final product was filtered, washed with distilled water, and dried at 373 K. Material was calcined at 823 K for 15 h under air for surfactant removal to obtain Zr-Nano-ZSM-5. Materials prepared with different Si/Zr ratio are represented as Zr-Nano-ZSM-5 (x), where $x = \text{Si}/\text{Zr}$ ratio.

Al-Nano-ZSM-5 (50) was synthesized by following the reported procedure using PrTES as an additive [39]. Conventional Zr-ZSM-5 (50) and Al-ZSM-5 (50) were synthesized using the similar procedure that was adopted for the preparation of Zr-Nano-ZSM-5 (50) and Al-Nano-ZSM-5 (50), respectively, but in the absence of PrTES. For comparative study, mesoporous Zr-KIT-6 and Zr-SBA-15 (50)

were prepared using ZrIPO by following the reported procedures [47,48].

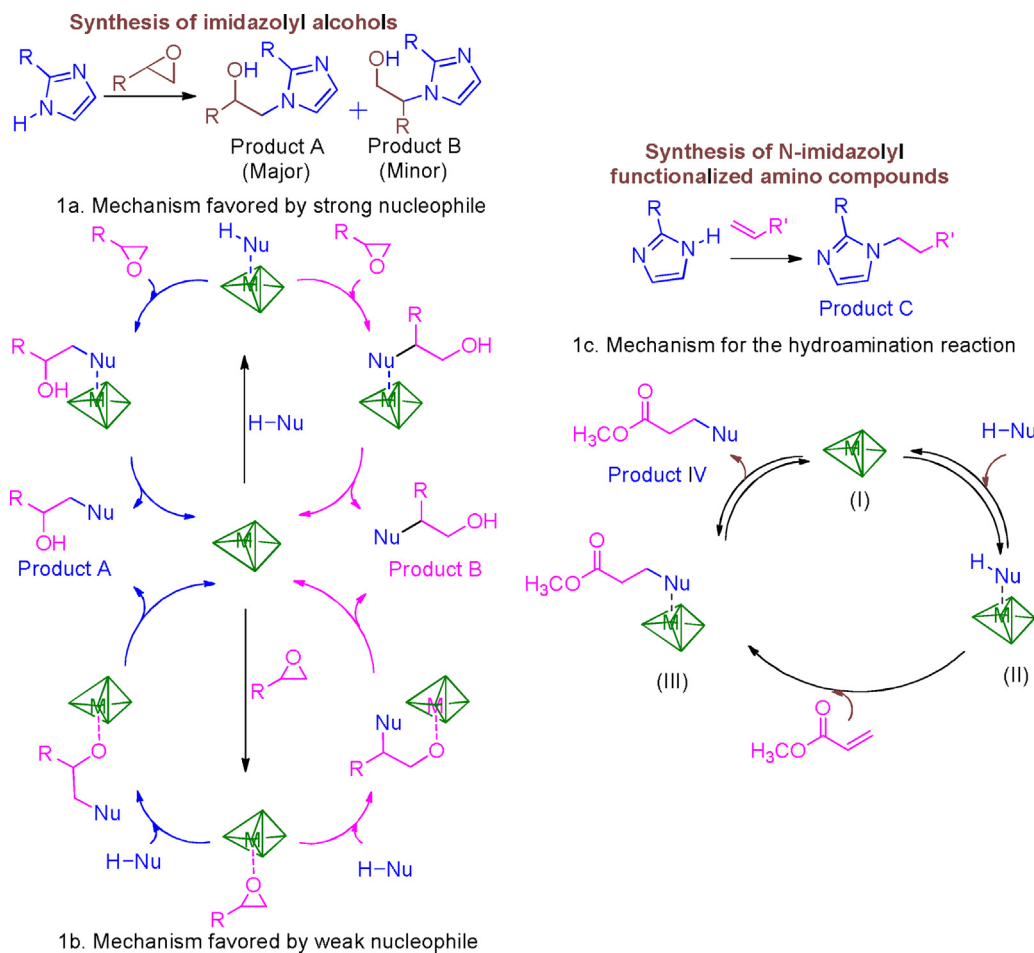
2.2. Material characterization

X-ray diffraction (XRD) patterns were recorded in the 2θ range of 5–60° for wide angle and 0.5–5° for low angle with a scan speed of 1°/min on a PANalytical X'PERT PRO diffractometer using Cu K α radiation ($\lambda = 0.1542 \text{ nm}$, 40 kV, 40 mA) and a proportional counter detector. N₂ adsorption measurements were performed at 77 K by Quantachrome Instruments Autosorb-IQ volumetric adsorption analyzer. Sample was out-gassed at 573 K for 3 h in the degas port of the adsorption apparatus. The specific surface area of zeolites was calculated from the adsorption data points obtained at P/P_0 between 0.05 and 0.3 using the Brunauer–Emmett–Teller (BET) equation. The pore diameter was estimated using the Barret–Joyner–Halenda (BJH) method. Scanning electron microscopy (SEM) measurements were carried out on a JEOL JSM-6610LV to investigate the morphology of the zeolites. The detailed TEM structural analysis of the developed morphologies were carried out using FEI, Tecnai G² F30, S-Twin microscope operating at 300 kV equipped with a GATAN Orius CCD camera. High-angle annular dark field scanning transmission electron microscopy (HAADF-STEM) employed here using the same microscope, which is equipped with a scanning unit and a HAADF detector from Fischione (model 3000). The compositional analysis was performed by energy dispersive X-ray spectroscopy (EDS, EDAX Instruments) attachment on the Tecnai G² F30. The sample was dispersed in ethanol using ultrasonic bath, mounted on a carbon coated Cu grid, dried, and used for TEM measurements. Acidity was examined by temperature-programmed desorption (TPD) with ammonia using a Quantachrome Autosorb-IQ. Before TPD experiments, catalyst was pre-treated in He (50 mL/min) at 873 K for 1 h. After cooling down to 343 K, a mixture of NH₃ in He (10:90) was passed (75 mL/min) at 343 K for 1 h. Then, the sample was subsequently flushed by He stream (50 cm³/min) at 373 K for 1 h to remove physisorbed ammonia. The TPD experiments were carried out in the range of 373–973 K at a heating rate of 10 K/min. The ammonia concentration in the effluent was monitored with a gold-plated, filament thermal conductivity detector. Fourier transform infrared (FTIR) spectra were recorded on a Bruker spectrophotometer in the region 400–4000 cm⁻¹ (spectral resolution = 4 cm⁻¹; number of scans = 200). Samples were prepared in the form of KBr pellets (1 wt.%). Diffuse reflectance UV-visible (DRUV-vis) measurements were conducted using a Shimadzu UV-2550 spectrophotometer equipped with an integrating sphere attachment (ISR 2200). Spectral grade BaSO₄ was used as a reference material. ¹H/¹³C NMR spectra were recorded on a JEOL (JNM-ECS400 Spectrometer; 400 MHz).

2.3. Procedure for catalytic reactions

For the synthesis of imidazolyl alcohols, equimolar amounts (5 mmol) of epoxide and imidazole were taken in a 50 mL round-bottomed flask. Required amount of catalyst was added to the reaction mixture and the reaction flask was placed in a temperature-controlled oil bath. The reaction flask was attached to a water-cooled condenser. The reaction was conducted at a specific temperature for a desired period of time. The progress of the reaction was monitored by gas chromatograph. Products were characterized by using various spectroscopic tools that matched well with the reported literature [13–17].

For the synthesis of other imidazole derivatives reported in this study, reactions were performed by reacting activated olefins (3 mmol) and imidazoles (2 mmol). A known amount of catalyst was added to the reaction mixture and reaction flask was placed in



Scheme 1. Proposed mechanism for the (a and b) ring opening of epoxide with strong/weak nucleophiles, and (c) hydroamination reaction over metallosilicate catalyst.

a temperature-controlled oil bath. The reaction flask was attached to a water-cooled condenser. The reaction was conducted at a specific temperature for a desired period of time. The progress of the reaction was monitored by gas chromatograph. Products were characterized by using various spectroscopic tools that matched well with the reported literature [19–31].

3. Results and discussion

3.1. Catalyst characterization

XRD patterns of M-Nano-ZSM-5 and conventional M-ZSM-5 samples were found to be identical and show the characteristic peaks of crystalline MFI framework structure (Fig. 1a) [39]. The low-angle XRD patterns of the mesoporous Zr-KIT-6 and Zr-SBA-15 samples are consistent with the reported literature (Fig. S1a) [47,48]. Furthermore, only a broad, wide-angle XRD patterns in the 2θ range of 22–26° were observed, which confirm that Zr-KIT-6 and Zr-SBA-15 are amorphous in nature.

Zr-Nano-ZSM-5 (50) exhibited type-IV isotherm similar to that of mesoporous materials (Fig. 1b). The major difference between Zr-Nano-ZSM-5 isotherm and Zr-ZSM-5 isotherm is a distinct increase of N_2 adsorption in the region $0.4 < P/P_0 < 0.9$, which is interpreted as a capillary condensation in mesopore void spaces. The mesopores show a broad pore size distribution in the range of 5–50 nm (inset of Fig. 1b). The N_2 -adsorption investigation reveals that the external surface area and pore volume of Zr-Nano-ZSM-5 (50) are much higher than that of conventional Zr-ZSM-5 (50) (Table 1). Zr-SBA-15 (50) and Zr-KIT-6 (50) samples exhibited type IV isotherms

with H1 hysteresis loops (Fig. S1b), which matched well with the reported literature [47,48]. Surface area and pore volume obtained from the sorption data are provided in Table 1.

Zr-ZSM-5 (50) exhibited capsule like morphology with a particle size of approximately 100 nm, whereas Zr-Nano-ZSM-5 (50) exhibited irregular aggregated nanoparticle morphology (Fig. S2). SEM image of Zr-SBA-15 (50) shows many wheat-like aggregated microstructures, whereas Zr-KIT-6 exhibited irregular flake like morphology (Fig. S2). Detailed nanostructure is already reported for the conventional M-ZSM-5, Zr-SBA-15, and Zr-KIT-6 [47,48]. Catalytic investigation (described below) confirms that Zr-Nano-ZSM-5 (50) exhibited the highest activity; therefore in-depth study was made for Zr-Nano-ZSM-5 (50) using HR-TEM.

TEM image of Zr-Nano-ZSM-5 (50) shows the irregular aggregated nanoparticle morphology with 10–20 nm particle size (Fig. 2a and b). To investigate the chemical composition of the dots and surrounding matrix, high-angle annular darkfield (HAADF) analysis was performed (Fig. 2c). It provides the Z-contrast image, where the intensity of scattered electrons is proportional to the square of the atomic number Z. EDX spectrum from a region marked by yellow area in Fig. 2c confirms the presence of O, Zr, and Si atoms (Fig. 2d). Comparison of concentrations across the structure was made by EDX line profile. The representative EDX line profile across the line shown in Fig. 2c shows the elemental distribution of Si, O, and Zr (Fig. 2e-h).

Zr-Nano-ZSM-5 (50) and Zr-ZSM-5 (50) exhibited UV absorption band in the range of 205–210 nm and a less distinguished overlapped absorption in the range of 215–230 nm (Fig. 1c). UV absorption band in the range of 205–210 nm is attributed

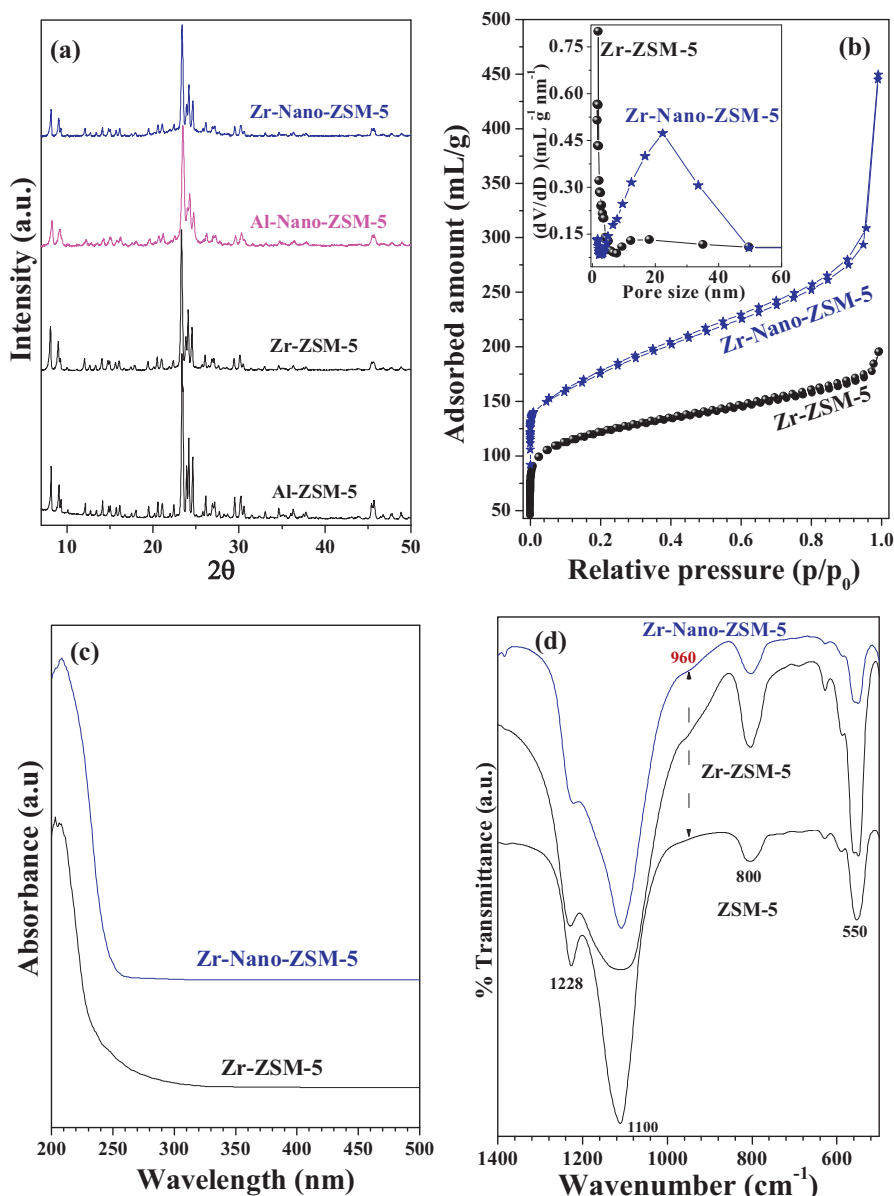


Fig. 1. (a) Wide angle XRD patterns, (b) N₂-adsorption isotherms (inset shows pore size distribution), (c) Diffuse reflectance UV-vis spectra, and (d) FT-IR spectra of Zr-Nano-ZSM-5 (50) and Zr-ZSM-5 (50).

to mono-atomically dispersed Zr⁴⁺ ions in tetra-coordinated geometry, whereas the absorption in the range of 215–230 nm corresponds to Zr(OH)(OSi)₃ structure [49]. These absorption bands arise due to ligand-to-metal (O²⁻ → Zr⁴⁺) charger transfer

transitions. The electronic transition for Zr(OH)(OSi)₃ occurs at lower energy (at higher wavelength) than that of Zr(OSi)₄ due to the differences in the electron donating capacities of OH⁻ and OSi⁻ ligand groups (electron donating capacity of HO⁻ > OSi⁻). Hence,

Table 1
Textural properties of metallosilicates synthesized in this work.

Materials	Si/M ^a		S _{BET} ^b (m ² /g)	Ext. SA (m ² /g)	V _{Total} (mL/g)	Total acidity ^c (mmol/g)
	Input	Output				
Al-ZSM-5 (50)	50	52.4	332	71	0.26	1.34
Al-Nano-ZSM-5 (50)	50	52.8	535	255	0.57	1.19
Zr-ZSM-5 (50)	50	61.5	463	130	0.27	0.77
Zr-Nano-ZSM-5 (50)	50	57.8	565	260	0.55	0.83
Zr-SBA-15 (50)	50	59.1	920	740	1.43	0.61
Zr-KIT-6 (50)	50	58.4	1040	810	1.78	0.65
Zr-Nano-ZSM-5 (50) (recycled catalyst)	50	58.5	542	256	0.51	0.85

^a Obtained by ICP analysis.

^b S_{BET} calculated from the adsorption data obtained in the region of $0.05 < P/P_0 \leq 0.3$.

^c Obtained by NH₃ TPD analysis.

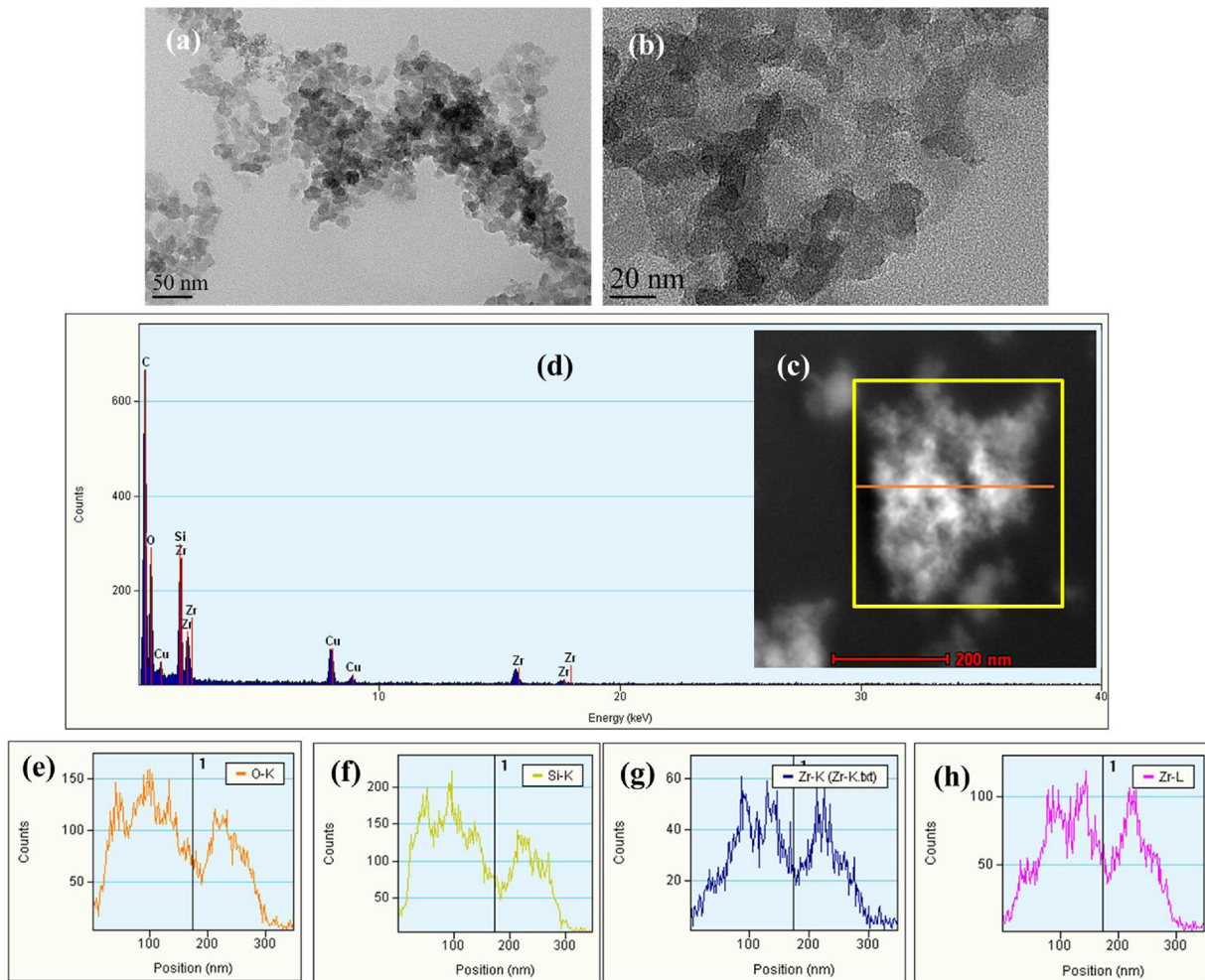


Fig. 2. (a and b) TEM image, (c) HAADF image, (d) EDX spectrum of the area highlighted in panel (c), and (e–h) EDX line profile of the line shown in panel (c) for Zr-Nano-ZSM-5 (50).

the energy gap between oxygen and Zr molecular orbitals is lower in the case of $\text{Zr}(\text{OH})(\text{OSi})_3$ than that of $\text{Zr}(\text{OSi})_4$. The UV absorption band of Zr-SBA-15 (50) and Zr-KIT-6 (50) samples matched well with the reported spectra [47,48]. These material exhibited UV absorbance in the range of 205–215 nm and a less distinguished overlapped absorption in the range of 215–250 nm. In addition to these absorptions, an additional weak absorption band centered at 280 nm was also observed for Zr-SBA-15/Zr-KIT-6, which can be correlated to extra framework ZrO_2 species [47,48].

FT-IR spectra of various materials investigated in this study exhibited common peaks at 800 cm^{-1} , 1100 cm^{-1} , and 1230 cm^{-1} (Fig. 1d) [50]. The absorption at 550 cm^{-1} observed in the case of M-Nano-ZSM-5 and M-ZSM-5 is due to the pentasil framework vibration of MFI framework structure. This peak was not observed in the FT-IR spectra of Zr-SBA-15 and Zr-KIT-6 (Fig. S1c). The absorption peak at 800 cm^{-1} is due to Si—O—Si symmetric stretching, and absorption peaks at 1100 cm^{-1} and 1230 cm^{-1} are assigned to asymmetric stretching of Si—O—Si. It may be noted that no FT-IR signal was observed at 960 cm^{-1} for Si-ZSM-5 sample. Whereas, a weak IR absorption at 960 cm^{-1} for Zr containing ZSM-5 materials and a sharp but low intense peak at 970 cm^{-1} was observed for Zr-SBA-15/Zr-KIT-6. This FT-IR peak confirmed the incorporation of metal ions in the framework structure and assigned to an asymmetric stretching mode of a $[\text{SiO}_4]$ unit bonded to a Zr^{4+} ion ($\text{O}_3\text{Si—O—Zr}$) [50].

Temperature programmed desorption of ammonia ($\text{NH}_3\text{-TPD}$) was employed to gain insights into the acidity of the solid materials investigated in this study (Table 1). As shown in Table 1, the acidity of Zr containing materials was found to be less than Al containing materials. The order of total acidity of various catalysts prepared with $\text{Si/M} = 50$ was found to be Al-ZSM-5 > Al-Nano-ZSM-5 > Zr-Nano-ZSM-5 > Zr-ZSM-5 > Zr-KIT-6 > Zr-SBA-15.

3.2. Catalytic activity

3.2.1. Synthesis of imidazolyl alcohols

Imidazolyl alcohols were synthesized by the ring opening of epoxide with imidazole (aminolysis reaction) in the presence of various catalysts prepared in this study (Table 2). To optimize the reaction condition, styrene oxide and imidazole were chosen. Two isomerized products A and B were obtained by the ring opening of styrene oxide with imidazole (Scheme 1). Under our reaction condition, only trace amount of product (<1%) was obtained in the absence of catalyst (Table 2). Both, the nature and type of the catalyst influenced the epoxide conversion and product selectivity. Zr-ZSM-5 (50) was found to be more active than Al-ZSM-5 (50), which is reverse the acidity order obtained from $\text{NH}_3\text{-TPD}$ (Table 2). This result suggests that Zr incorporation in the framework is favorable for the synthesis of imidazolyl alcohols by the ring opening reaction of epoxide. Nanocrystalline ZSM-5 materials

Table 2

Comparative catalytic activity of various metallosilicates in the synthesis of imidazolyl alcohols.



E. N.	Catalyst	Nucleophile (R)	Epoxide	Conv. (%)	Product sel. (%)		Average TOF (h^{-1})
					A	B	
1	None	H	R' = Ph	<1%	—	—	—
2	Al-ZSM-5 (50)	H	R' = Ph	8	63	37	68
3	Al-Nano-ZSM-5 (50)	H	R' = Ph	15	62	38	131
4	Zr-ZSM-5 (50)	H	R' = Ph	49	83	17	491
5	Zr-Nano-ZSM-5 (30)	H	R' = Ph	96	88	12	576
6	Zr-Nano-ZSM-5 (50)	H	R' = Ph	82	88	12	774
7	Zr-Nano-ZSM-5 (100)	H	R' = Ph	61	86	14	1084
8	Zr-SBA-15 (50)	H	R' = Ph	31	81	19	298
9	Zr-KIT-6 (50)	H	R' = Ph	30	82	18	285
10	Zr-Nano-ZSM-5 (50)	CH ₃	R' = Ph	52	84	16	491
11	Zr-Nano-ZSM-5 (50)	H	R' = CH ₃	31 ^a	90	10	293
12	Zr-Nano-ZSM-5 (50)	H	R' = Ph	43 ^a	88	12	406
13	Zr-Nano-ZSM-5 (50) ^b	H		78		736	

Reaction conditions: catalyst (25 mg), imidazole (5 mmol), styrene oxide (5 mmol), reaction temperature (318 K), reaction time (45 min).

Average TOF (h^{-1}) = Turnover frequency [moles of styrene oxide converted per mole of active metal (Zr/Al) per hour].

^a Reaction temperature (303 K).

^b Only one product was obtained.

exhibited higher catalytic activity than that of conventional ZSM-5 materials. Among all ZSM-5 materials investigated in this study, Zr-Nano-ZSM-5 exhibited the highest catalytic activity. Intercrystalline mesopores and large external surface area of nanocrystalline ZSM-5 provide better accessibility of the reactant molecules to the active sites and facile diffusion of product molecules through mesopores, compared to the conventional ZSM-5 materials. Further catalytic investigation reveals that amorphous mesoporous Zr-SBA-15 (50) and Zr-KIT-6 (50) exhibited less activity than Zr-Nano-ZSM-5 (50). This result confirms that Zr incorporation in the crystalline zeolite framework is required for high activity.

Influence of reaction parameters such as role of solvent, reaction temperature, amount of catalyst, Si/Zr ratio were investigated by taking Zr-Nano-ZSM-5 (50) as a catalyst, styrene oxide and imidazole as model substrates. Catalytic activity of Zr-Nano-ZSM-5 (50) was found to be significantly higher in the absence of solvent, when compared to the reactions performed in a solvent medium (Table S1). This reduction in the catalytic activity can be correlated to the competitive adsorption of reactant and solvent molecules. This competitive adsorption creates obstacle for the reactant molecules to reach active sites in the presence of solvent molecule; therefore, catalytic activity was decreased. When the reaction was performed under solvent free condition, only reactant molecules are accessible to the active sites and high catalytic activity was achieved. With increase in the temperature from 303 to 333 K, conversion of styrene oxide increased from 43 to 94 mol% (Fig. S3). Amount of catalyst influences the conversion of styrene oxide. With increase in the amount of catalyst, epoxide conversion increased (Fig. S3). However, when average TOF was taken into account, catalytic activity obtained with 25 mg of catalyst was found to be better than that of 50 mg of catalyst for 5 mmol of styrene oxide. Influence of Si/Zr molar ratio shows that catalyst prepared with high Si/Zr ratio exhibited higher activity (Compare average TOF of entries 5–7, Table 2). This result confirmed that all Zr sites present in the catalyst (prepared with high Si/Zr) are involved in the reaction. The comparative catalytic activity data summarized in Table 3 shows that nanocrystalline Zr-Nano-ZSM-5 investigated in this study

exhibited significantly higher activity than various catalysts reported in the literature for the aminolysis reaction of imidazole with styrene oxide.

It is known in the literature that Lewis acid catalyst provides good selectivity for amino alcohol A, when strong nucleophile is used. Strong nucleophile attacks the least hindered carbon of epoxide and follows S_N2 mechanism to produce amino alcohol A. In contrast, high selectivity for amino alcohol B was obtained when weak nucleophile was reacted with epoxide. Weak nucleophiles are susceptible to attack on the stable carbocation formed by the epoxide (Scheme 1a and b) [15]. To evaluate the scope of this reaction for the synthesis of a wide range of imidazolyl alcohols, various epoxides (propylene oxide, cyclohexene oxide, and styrene oxide) and imidazoles (imidazole and 2-methyl imidazole) were chosen. Order of catalytic activity for imidazole and various epoxides follows the order: styrene oxide > cyclohexene oxide > propylene oxide (Table 4). When the reaction of styrene oxide with various amines was analyzed, it was found that the reactivity and selectivity can be correlated with the basicity of the amines (strong nucleophiles/higher basic amines have higher pK_a value) (Table 4). Strong nucleophiles produced high selectivity for product A (but with low average TOF), whereas weak nucleophiles produced high selectivity for product B (with high average TOF). The reactivity difference can be explained by the competitive adsorption of amines and styrene oxide over Zr-Nano-ZSM-5 (50) (Table 4). FT-IR provides evidence that imidazole is preferentially adsorbed on the catalyst surface during the ring opening reaction of imidazole and styrene oxide (Fig. S4). When the relative adsorption ratio of amine/styrene oxide was found to be greater than 2, then product A was found in higher selectivity than product B. Competitive adsorption study provides evidence for the difference in the product selectivity observed for weak and strong nucleophiles (Table 4). In the first step, strong nucleophiles (for example imidazole) adsorbed on the active sites and the adsorbed nucleophiles attack on the less hindered side of styrene oxide (either adsorbed or present in the bulk) to form more selective product A. While, in the case of weak nucleophile (aniline), it was less adsorb on the active sites when compared to

Table 3

Comparative catalytic activity data for the aminolysis and hydroamination reactions over various catalysts reported in the literature with Zr-Nano-ZSM-5 (50).

Ring opening reaction of styrene oxide with imidazole					
E. No.	Catalyst	Solvent	Temp./time	Styrene oxide conv. (%)	Lit. Ref.
1	SiO ₂ with high pressure (10 kbar)	CH ₃ CN	RT/7 days	47	[14]
2	High pressure (10 kbar)	CH ₃ CN	338 K/3 days	60	[15]
3	Y(NO ₃) ₃ ·6H ₂ O	Neat	RT/24 h	90	[17]
4	Microwave irradiation (360/510 W)	Neat	360/510 W with pressure	60	[16]
5	Steps involved: (a) silylation, (b) LiBr, and (c) desilylation with KF	CH ₃ OH	333 K/6 h followed by RT/3 h	78	[18]
6	Zr-Nano-ZSM-5 (50)	Neat	318 K/45 min	96	This work

Hydroamination reaction of imidazole with methyl acrylate					
E. No.	Catalyst	Solvent	Temp./time	Yield of product [C] (%)	Lit. Ref.
1	KF/Al ₂ O ₃	CH ₃ CN	RT/18 h	96	[19]
2	[Ti ₄ H ₁₁ (PO ₄) ₉]·nH ₂ O	Neat	323 K/6 h	85	[24]
3	Bmim]OH	Neat	RT/6 h	90	[26]
4	[Bmim]Im	Neat	RT/1 h	93	[27]
5	Cu(acac) ₂ in [bmim][BF ₄]	Neat	333 K/8 h	90	[28]
6	PS-imCuI	DMF	348 K/4 h	90	[29]
7	DBU	CH ₃ CN	RT/14 h	95	[25]
8	[DBU]-derived ionic liquid	Neat	RT/2 h	0	[30]
9	Y(NO ₃) ₃ ·6H ₂ O	Neat	RT/24 h	90	[20]
10	Vanadyl(IV) acetate	Neat	RT/45 min	92	[21]
11	I ₂	CH ₂ Cl ₂	RT/9 h	50	[22]
12	Silica-supported AlCl ₃	Neat	333 K/4 h	52	[23]
13	PEG-400 as solvent	0.5 mL of PEG-400	RT/6.5 h	89	[31]
14	Zr-Nano-ZSM-5 (50)	Neat	318 K/5 min	96	This work

styrene oxide. Styrene oxide is adsorbed on the active acid sites to form stable carbocation, which was attacked by the weak nucleophile (either adsorbed or present in solution) to form product B in the high selectivity. As shown in Table 4, strong nucleophile (having $pK_a > 7$) such as imidazole, butylamine, and cyclohexylamine afforded high selectivity for product A, while weak nucleophile ($pK_a < 7$) such as aniline afforded higher selectivity for product B.

Further, the aminolysis reaction of styrene oxide (5 mmol) with equimolar amount of imidazole (2.5 mmol) and 2-methyl imidazole (2.5 mmol) was investigated. Table 5 shows that aminolysis products (6+7) selectivity obtained by the reaction of imidazole and styrene oxide was found to be more than the products (8+9) selectivity obtained by the reaction on 2-methyl imidazole and styrene oxide. This confirms the high reactivity of imidazole when compared to 2-methylimidazole. Similarly,

Table 4

Competitive adsorption of styrene oxide & various nucleophiles (along with pK_a) at Zr-Nano-ZSM-5 (50) and the catalytic activity for the ring opening reaction of styrene oxide with these nucleophiles.

Adsorbent	Amount adsorbed mmol/g catalyst	Relative adsorption ratio: amine/SO		Average TOF (h ⁻¹)	Product selectivity (%)	pK_a value of amine
		Amine	SO			
(SO + Nu)						
	0.56	0.04	14.0	774 ^a	88	12
	0.38	0.17	2.2	101 ^a	86	14
	0.36	0.17	2.1	100 ^a	85	10.6
	0.14	0.18	0.77	7040 ^b	4	96

25 mg of Zr-Nano-ZSM-5 (50) was suspended for 15 min in equimolar amounts (1 mmol) of styrene oxide (SO), amines as a nucleophile (Nu) dissolved in 5 mL of dichloromethane as a solvent and addition n-decane (1 mmol) used for standard. The catalyst was, then, separated and the concentration of the substrate in the liquid portion was determined by gas chromatography. The amount adsorbed on the catalyst surface was determined by difference.

Average TOF (h⁻¹) = Turnover frequency [moles of epoxide converted per mole of active Zr per hour].

^a Average TOF at 318 K after 45 min of the reaction.

^b Average TOF at 318 K after 5 min of the reaction.

Table 5

Competitive aminolysis reactions of substituted imidazole and epoxides over Zr-Nano-ZSM-5 (50).

Nucleophiles	Epoxides	Products			
(1), R=H (2), R=CH ₃	Ph-CH ₂ -O-CH ₂ -Ph (3) H ₃ C-CH ₂ -O-CH ₂ -CH ₃ (4) Cyclohexene oxide (5)	Ph-CH(OH)-N(R)-imidazole (6), R=H (8), R=CH ₃	Ph-CH(OH)-CH ₂ -N(R)-imidazole (7), R=H (9), R=CH ₃	OH-CH ₂ -N(R)-imidazole (10) OH-CH ₂ -CH ₂ -N(R)-imidazole (11)	.
Nucleophiles (mmol)	Epoxides (mmol)	Conv. (%)	Product selectivity (%)		
(1)	(2)	(3)	(4)	(5)	(6)+(7) (8)+(9) (10)+(11) (12)
2.5	2.5	5.0	—	—	42 61 39 —
5	—	2.5	2.5	—	21 ^a 55 — 45
5	—	2.5	—	2.5	41 52 — — 48

Reaction conditions: Zr-Nano-ZSM-5 (50) (25 mg), reaction temperature (318 K), reaction time (45 min).

Average TOF (h⁻¹) = Turnover frequency [moles of epoxide converted per mole of active metal Zr per hour].

^a Reaction temperature (303 K).

aminolysis reaction of imidazole (5 mmol) with equimolar amount of styrene oxide (2.5 mmol) and propylene oxide/cyclohexene oxide (2.5 mmol) was investigated. Catalytic activity data shown in Table 5 confirms that the different ratio of the observed products is due to the different reactivity of epoxides. Reactivity of propylene oxide is less compared to styrene oxides, therefore more selectivity was observed for the products obtained from the aminolysis reaction of styrene oxide and imidazole when compared to propylene oxide and imidazole. Based on the amount of products obtained by the aminolysis reaction of imidazole and styrene oxide/cyclohexene oxide, one can conclude that both epoxides have almost similar reactivity toward imidazole.

3.2.2. Synthesis of *N*-imidazolyl functionalized β -amino compounds

A wide range of imidazole derivatives can be synthesized by the hydroamination reaction of imidazole and activated olefins (Scheme 1). The conjugate addition of imidazole and methyl acrylate was investigated over various catalysts prepared in this study (Table 6). The order of catalytic activity of various catalysts was found to be Zr-Nano-ZSM-5 (50) > Zr-ZSM-5 (50) > Zr-SBA-15 (50) ≈ Zr-KIT-6 (50) > Al-Nano-ZSM-5 (50) > Al-ZSM-5 (50). This observation confirmed that, Zr incorporation in the crystalline zeolite framework is ideally suited for the synthesis of imidazole derivatives. Influence of reaction parameters such as role of solvent, reaction temperature, amount of catalyst, Si/Zr ratio was investigated by taking Zr-Nano-ZSM-5 (50) as a catalyst, methyl acrylate and imidazole as model substrates. The catalytic activity of Zr-Nano-ZSM-5 (50) was found to be more when reaction was performed in the absence of solvent (Table S2). Solvent molecules, especially polar solvent molecules can block the active sites due to the competitive adsorption of reactant and solvent molecules. This competitive adsorption creates hindrance for the reactant molecules to reach active sites in the presence of solvent molecules; therefore, low catalytic activity was observed. With increase in the temperature from 298 to 333 K, reaction yield was increased from 18 to 99 mol% (Fig. S5). It is interesting to note that unlike the conventional process, the reaction of methyl acrylate with imidazole occurs even at ambient conditions (298 K). Amount of catalyst also influences the reaction yield. With increase in the amount of catalyst, product yield also increased (Fig. S5). When average TOF was taken into account, 25 mg of catalyst exhibited better activity than that of 50 mg of catalyst for 2 mmol of reactants. Influence of Si/Zr molar ratio was investigated and it was found that materials prepared with high Si/Zr exhibited higher activity (Compare average

TOF of entries 5–7, Table 6). The comparative catalytic activity data summarized in Table 3 shows that nanocrystalline Zr-Nano-ZSM-5 investigated in this study is more active than various catalysts reported in the literature for the hydroamination reaction of methyl acrylate with imidazole.

Imidazole is activated at the acid sites of zeolite (I) in the first step to form intermediate (II) by acid-base interaction, followed by Michael addition of methyl acrylate to give the intermediate (III) (Scheme 1c). The intermediate (III), then, releases the anti-adduct (product IV) to regenerate acid sites of the catalyst (I). Let's assume that methyl acrylate is adsorbed at acid sites of zeolite catalyst, which is followed by the formation of corresponding cation. In this mechanism, unfortunately, nucleophile (imidazole) attacks preferentially to the α -carbon of methyl acrylate to give Markovnikov adduct. But this second possibility is ruled out in our study, because no Markovnikov adduct was formed. Since our catalyst is an acid catalyst, therefore, the adsorption of imidazole on acid sites of zeolite by acid-base interaction is more appropriate (and does occur as shown above in the competitive adsorption studies) than that of methyl acrylate to yield acrylate cation.

To evaluate the scope of this methodology for the synthesis of wide range of imidazole derivatives, imidazole/2-methylimidazole was reacted with various activated olefins (Table 6). Reactions of imidazole with methyl acrylate, ethyl acrylate, and acrylonitrile produced almost similar yields of the corresponding products. However, less product yield was observed when the reaction was performed with 2-cyclohexenone. Significantly, longer reaction time is required for the hydroamination reaction of ethyl cinnamate. Furthermore, the product yield was less when 2-methyl imidazole was reacted with methyl acrylate when compared with product yield obtained using imidazole. The result confirms that the reaction is influenced by the reactivity of the substrate. Imidazole ($pK_a = 14.5$) having high pK_a value offered high yield of desired product when compared to 2-methylimidazole ($pK_a = 7.86$).

The competitive hydroamination reactions of various amines with different olefins were investigated. Depending on amine and olefin reactivity, selectivity of the product varies. For example, equimolar amounts of aniline (1.0 mmol) and imidazole (1.0 mmol) were reacted with methyl acrylate (2 mmol) in the presence of Zr-Nano-ZSM-5 (50). After 5 min, only N-alkylation of imidazole was obtained exclusively with 72% conversion of methyl acrylate and 100% selectivity (entry No. 2, Table 7). It is highly probable that aniline chemisorbs on some acid sites that is responsible for the reduction of product yield. Under the reaction condition, no aniline derived product was observed. However, when aniline was reacted

Table 6

Comparative catalytic activity of various metallosilicates in the hydroamination reaction.

Entry No.	Catalyst	Nucleophile (R)	Acceptor	Yield of product [C] (%)	Average TOF (h ⁻¹)
1	None	H		–	–
2	Al-ZSM-5 (50)	H		19	585
3	Al-Nano-ZSM-5 (50)	H		31	955
4	Zr-ZSM-5 (50)	H		52	1870
5	Zr-Nano-ZSM-5 (30)	H		96	2073
6	Zr-Nano-ZSM-5 (50)	H		81	3250
7	Zr-Nano-ZSM-5 (100)	H		58	3708
8	Zr-SBA-15 (50)	H		42	1453
9	Zr-KIT-6 (50)	H		43	1474
10	Zr-Nano-ZSM-5 (50)	CH ₃		59	2367
11	Zr-Nano-ZSM-5 (50)	H		83	3330
12	Zr-Nano-ZSM-5 (50)	H		84	3370
13	Zr-Nano-ZSM-5 (50)	H		67 ^a	19
14	Zr-Nano-ZSM-5 (50)	H		53	2126

Reaction conditions: catalyst (25 mg), imidazole (2 mmol), methyl acrylate (2 mmol), reaction temperature (318 K), reaction time (5 min).

Average TOF (h⁻¹) = Turnover frequency [moles of imidazole converted per mole of active metal (Zr/Al) per hour].

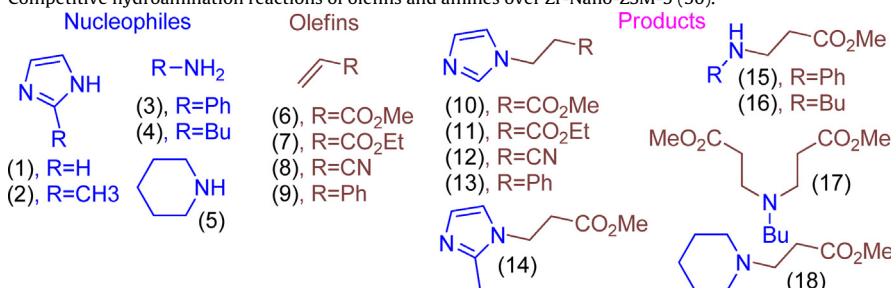
^a Reaction temperature (353 K), time (12 h). [C] = N-imidazolyl functionalized β-amino compounds.

with methyl acrylate at 353 K for 12 h, almost quantitative yield of the product was obtained. These investigations confirm that rate of the reaction of imidazole with methyl acrylate is very high when compared to the rate of the reaction of aniline with methyl acrylate.

Within the small reaction time (5 min), aniline was not able to form the product. It may be noted that, equimolar amounts of styrene and methyl acrylate were reacted to imidazole (2 mmol) in the presence of Zr-Nano-ZSM-5 (50), and then only hydroamination product

Table 7

Competitive hydroamination reactions of olefins and amines over Zr-Nano-ZSM-5 (50).



Nucleophile (mmol)					Olefins (mmol)				Conv. (%)	Product selectivity (%)							
(1)	(2)	(3)	(4)	(5)	(6)	(7)	(8)	(9)	10	11	12	13	14	15	16	17	18
1	1	–	–	–	2	–	–	–	67	55	–	–	45	–	–	–	–
1	–	1	–	–	2	–	–	–	72	100	–	–	–	0	–	–	–
1	–	–	1	–	2	–	–	–	96	7	–	–	–	–	60	33	–
1	–	–	–	1	2	–	–	–	97	10	–	–	–	–	–	–	90
2	–	–	–	–	1	1	–	–	77	48	52	–	–	–	–	–	–
2	–	–	–	–	1	–	1	–	78	46	–	54	–	–	–	–	–
2	–	–	–	–	1	–	–	1	40	100	–	–	0	–	–	–	–

Reaction conditions: Zr-Nano-ZSM-5 (50) (25 mg), reaction temperature (318 K), reaction time (5 min).

corresponding to the reaction of imidazole and methylacrylate was obtained. This confirms the sluggish rate of the reaction of styrene with imidazole. Several such examples are provided in Table 7.

Recyclability of Zr-Nano-ZSM-5 (50) was investigated in the aminolysis reaction of imidazole with styrene oxide and the hydroamination reaction of imidazole and methyl acrylate. At the end of each cycle, 5 mL of dichloromethane was added and the catalyst was separated by centrifugation, dried at 373 K and then used in the next cycle. Recycling experiments confirmed that no significant loss in the activity was observed after 5 recycles (Fig. S6). ICP analysis confirmed that Zr was not leached during the reaction. Textural characterizations using XRD and surface area analysis confirmed that the catalyst is stable.

Nanocrystalline ZSM-5 was obtained by the addition of PrTES in the synthesis composition of conventional ZSM-5. PrTES contains only three hydrolysable moieties with one hydrophobic alkyl group that are unfavorable for the formation of extended tetrahedral SiO_2 linkages. Consequently, the zeolite growth is significantly retarded at the organic and inorganic interfaces, resulting in the formation of aggregated ZSM-5 zeolite nanocrystals as observed in the TEM images (Fig. 2). Mesopores in zeolites are formed due to the crystal packing of these nanosized zeolite particles. Catalytic activities in the ring opening of epoxide with strong/weak amine nucleophiles and hydroamination reaction of activated olefins with imidazole suggest that isomorphous substitution of Zr in the zeolite MFI framework is responsible for the high activity. Acidity measurements confirmed that zeolites with high acidity are not suitable for these reactions. When acidity and activity are taken into the consideration for Al incorporated ZSM-5 materials and Zr incorporated ZSM-5 materials, one can conclude that fine tuning in the acidity by incorporating suitable metal ion in the MFI-framework is the required for these reactions. It seems that Zr incorporation provides optimum acidity for these reactions. Due to large ionic radius (0.73 Å for Zr^{4+} and 0.54 Å for Al^{3+}) and larger electronegative difference between M^{4+} and oxygen attached to epoxide ring (2.11 and 1.8 for O–Zr and O–Al, respectively), zirconosilicates can polarize the O–Zr bond more efficiently. The high polarizability of zirconosilicates is responsible for the weakening of O–C bond (of epoxide ring) and facile reaction of amine to epoxide to form desired product.

4. Conclusions

Nanocrystalline Zr-Nano-ZSM-5 prepared using propyltriethoxy silane exhibited large external surface area, mesopore volume, and possess intercrystalline mesopores. Zr-Nano-ZSM-5 exhibited exceptionally high catalytic activity compared to catalysts reported in the literature for the synthesis of imidazolyl alcohols and N-imidazolyl functionalized β -amino compounds. Based on catalytic activity, acidity measurements, adsorption experiments, and textural properties, one can conclude that optimum Zr polarizability, acidity, large external surface area, and intercrystalline mesopores are responsible for such a high activity of Zr-Nano-ZSM-5. Therefore, it can be concluded that by fine tuning of textural and acidic properties, it is possible to develop a highly efficient catalyst for a particular type of reaction.

Acknowledgements

Authors are thankful to DST for financial assistance through DST project SB/S1/PC-91/2012. R.K. is grateful to CSIR, New Delhi for SRF fellowship. We acknowledge Director, IIT Ropar for constant encouragements.

Appendix A. Supplementary data

Supplementary data associated with this article can be found, in the online version, at <http://dx.doi.org/10.1016/j.apcata.2014.03.006>.

References

- [1] V.F.D. Álvaro, A.F. Brigas, E.G. Derouane, J.P. Lourenço, B.S. Santos, *J. Mol. Catal. A: Chem.* 305 (2009) 100–103.
- [2] M.R. Grimmet, in: A.R. Katritzky, C.W. Rees, E.F.V. Scriven (Eds.), *Comprehensive Heterocyclic Chemistry II*, Pergamon, Oxford, 1996, pp. 77–220.
- [3] M. Botta, F. Corelli, F. Gasparrini, F. Messina, C. Mugnaini, *J. Org. Chem.* 65 (2000) 4736–4739.
- [4] T. Eicher, S. Hauptmann, *The Chemistry of Heterocycles*, Georg Thieme Verlag, New York, 1995.
- [5] D.M. Gabriella, L.R. Giuseppe, P. Di Alessandra, R. Rino, B. Alberto, C. Chiara, S. Anna, M. Giovanni, C. Emmanuele, A. Marino, S. Romano, *J. Med. Chem.* 48 (2005) 4378–4388.
- [6] R. Kore, R. Srivastava, *J. Mol. Catal. A: Chem.* 376 (2013) 90–97.
- [7] R. Kore, T.J. Dhipil Kumar, R. Srivastava, *J. Mol. Catal. A: Chem.* 360 (2012) 61–70.
- [8] R. Kore, R. Srivastava, *J. Mol. Catal. A: Chem.* 345 (2011) 117–126.
- [9] R. Kore, R. Srivastava, *Tetrahedron Lett.* 53 (2012) 3245–3249.
- [10] D. Joseph, K. Mukesh, Z. Matthias, T.P. Elizabeth, *Organometallics* 32 (2013) 966–979.
- [11] P.L. Arnold, M. Rodden, K.M. Davis, A.C. Scarisbrick, A.J. Black, C. Wilson, *Chem. Commun.* (2004) 1612–1613.
- [12] R. Kore, M. Tumma, R. Srivastava, *Catal. Today* 198 (2012) 189–196.
- [13] S. Tang, G.A. Baker, H. Zhao, *Chem. Soc. Rev.* 41 (2012) 4030–4066.
- [14] H. Kotsuki, K. Hayashida, T. Shimanouchi, H. Nishizawa, *J. Org. Chem.* 61 (1996) 984–990.
- [15] H. Kotsuki, M. Wakao, H. Hayakawa, T. Shimanouchi, M. Shiro, *J. Org. Chem.* 61 (1996) 8915–8920.
- [16] H. Desai, B.R. D’Souza, D. Foether, B.F. Johnson, H.A. Lindsay, *Synthesis* 6 (2007) 902–910.
- [17] M.J. Bhanushali, N.S. Nandurkar, M.D. Bhor, B.M. Bhanage, *Tetrahedron Lett.* 49 (2008) 3672–3676.
- [18] M.A. Jalila, S.M. Masum, *Tetrahedron Lett.* 53 (2012) 3049–3051.
- [19] J. Nath, M.K. Chaudhur, *Tetrahedron Lett.* 46 (2005) 3279–3282.
- [20] M.J. Bhanushali, N.S. Nandurkar, S.R. Jagtap, B.M. Bhanage, *Catal. Commun.* 9 (2008) 1189–1195.
- [21] R. Trivedi, P. Lalitha, S. Roy, *Synth. Commun.* 38 (2008) 3556–3566.
- [22] K.J. Borah, M. Phukan, R. Borah, *Synth. Commun.* 40 (2010) 2830–2836.
- [23] M.R. Saidi, Y. Pourshojaei, F. Aryanasab, *Synth. Commun.* 39 (2009) 1109–1119.
- [24] J. Nath, M.K. Chaudhur, *Catal. Lett.* 133 (2009) 388–393.
- [25] C.E. Yeom, M.J. Kim, B.M. Kim, *Tetrahedron* 63 (2007) 904–909.
- [26] L. Yang, L.W. Xu, W. Zhou, L. Li, C.G. Xia, *Tetrahedron Lett.* 47 (2006) 7723–7726.
- [27] X. Chen, X. Li, H. Song, Y. Qian, F. Wang, *Tetrahedron Lett.* 52 (2011) 3588–3591.
- [28] M. Lakshmi Kantam, B. Neelima, C.V. Reddy, R. Chakravarti, *Ind. Eng. Chem. Res.* 46 (2007) 8614–8619.
- [29] L. Li, Z. Liu, Q. Ling, X. Xing, *J. Mol. Cat. A: Chem.* 353–354 (2012) 178–184.
- [30] A.G. Ying, L. Liu, G.F. Wu, G. Chen, X.Z. Chen, W.D. Ye, *Tetrahedron Lett.* 50 (2009) 1653–1657.
- [31] D. Kumar, G. Patel, B.G. Mishra, R.S. Varma, *Tetrahedron Lett.* 49 (2008) 6974–6976.
- [32] M.E. Davis, *Nature* 417 (2002) 813–821.
- [33] F. Schütt, W. Schmidt, *Adv. Mater.* 14 (2002) 629–638.
- [34] C.S. Cundy, P.A. Cox, *Chem. Rev.* 103 (2003) 663–701.
- [35] R. Kore, B. Satpati, R. Srivastava, *Chem. Eur. J.* 17 (2011) 14360–14365.
- [36] R. Kore, B. Satpati, R. Srivastava, *ACS Catalysis* 3 (2013) 2891–2904.
- [37] R. Kore, R. SridharKrishna, R. Srivastava, *RSC Advances* 3 (2013) 1317–1322.
- [38] R. Kore, R. Srivastava, *RSC Advances* 2 (2012) 10072–10084.
- [39] R. Srivastava, N. Iwasa, S.-I. Fujita, M. Arai, *Chem. Eur. J.* 14 (2008) 9507–9511.
- [40] R. Srivastava, M. Choi, R. Ryoo, *Chem. Commun.* (2006) 4489–4491.
- [41] M. Choi, H.S. Cho, R. Srivastava, C. Venkatesan, D.H. Choi, R. Ryoo, *Nat. Mater.* 5 (2006) 718–723.
- [42] Y. Tao, H. Kanoh, L. Abrams, K. Kaneko, *Chem. Rev.* 106 (2006) 896–910.
- [43] J. Pérez-Ramírez, C.H. Christensen, K. Egeblad, C.H. Christensen, J.C. Groen, *Chem. Soc. Rev.* 37 (2008) 2530–2542.
- [44] C.H. Jacobsen, C. Madsen, J. Houzvicka, I. Schmidt, A. Carlsson, *J. Am. Chem. Soc.* 122 (2000) 7116–7117.
- [45] K. Egeblad, C.H. Christensen, M. Kustova, C.H. Christensen, *Chem. Mater.* 20 (2008) 946–960.
- [46] K. Na, C. Jo, J. Kim, K. Cho, J. Jung, Y. Seo, R.J. Messinger, B.F. Chmelka, R. Ryoo, *Science* 333 (2011) 328–332.
- [47] A. Ramanathan, B. Subramiam, R. Maheswari, U. Hanefeld, *Microporous Mesoporous Mater.* 167 (2013) 207–212.
- [48] D.M. Do, S. Jaenicke, G.K. Chuah, *Catal. Sci. Technol.* 2 (2012) 1417–1424.
- [49] P. Ratnasamy, D. Srinivas, H. Knözinger, *Adv. Catal.* 48 (2004) 1–169.
- [50] R. Szostak, *Molecular Sieves: Principles of Synthesis and Identification*, Van Nostrand Reinhold, New York, 1989, pp. 317.